Cao et al. Biochar (2026) 8:29
https://doi.org/10.1007/s42773-025-00546-z

Biochar

ORIGINAL RESEARCH Open Access

Pyrolysis temperature determines aging effects on the electron transfer and exchange properties of pyrogenic carbon

Mulin Cao[1,3†], Hao Ren[1†], Pengxiang Zhu[1], Wenmei Tao[4], Wei Du[1], Hao Li[1], Yandi Hu[2,3], Peng Zhang[1,3*] and Bo Pan[1,3*]

Abstract

Pyrogenic carbon (PyC) possesses electron transfer and exchange capabilities that can facilitate redox reactions in various geochemical and biochemical processes. The long-term environmental persistence of PyC makes it susceptible to substantial alterations in its physical and chemical properties through aging. However, there is a lack of research on how aging impacts PyC's electron transfer and exchange properties. This study investigated the effects of aging on PyC samples derived from four feedstocks and prepared at two different pyrolysis temperatures. Three aging methods, including chemical aging, freeze–thaw cycling, and natural aging over a year, were employed. The results indicate that aging significantly enhanced the conductivity of certain PyC samples produced at 350 °C by more than three orders of magnitude, potentially attributed to the enrichment of redox-active functional groups. Conversely, for PyC produced at 750 °C, aging damaged the polyaromatic carbon matrices, resulting in reduced conductivity. Aging was found to decrease the electron-donating capacity (EDC) while increasing the electron-accepting capacity (EAC) of PyC produced at 350 °C, primarily due to a reduction in electron-donating C–OH groups and an increase in electron-accepting O–C=O groups. These findings shed light on the aging effects on the electron transfer and exchange properties of PyC and offer valuable insights for assessing PyC's role in biogeochemical processes.

Highlights

- Aging significantly enhanced the conductivity of PyC produced at 350 °C.
- Aging damaged the polyaromatic carbon matrices and reduced the conductivity of PyC produced at 750 °C.
- Aging led to lower EDC and higher EAC by converting C–OH to O–C=O of PyC produced at 350 °C.

Keywords Pyrogenic carbon, Aging, Conductivity, Electron transfer properties, Polyaromatic carbon matrices

†Mulin Cao and Hao Ren contributed equally to this work.

*Correspondence:
Peng Zhang
da.feipeng@163.com
Bo Pan
panbocai@gmail.com
Full list of author information is available at the end of the article

Springer

Graphical Abstract

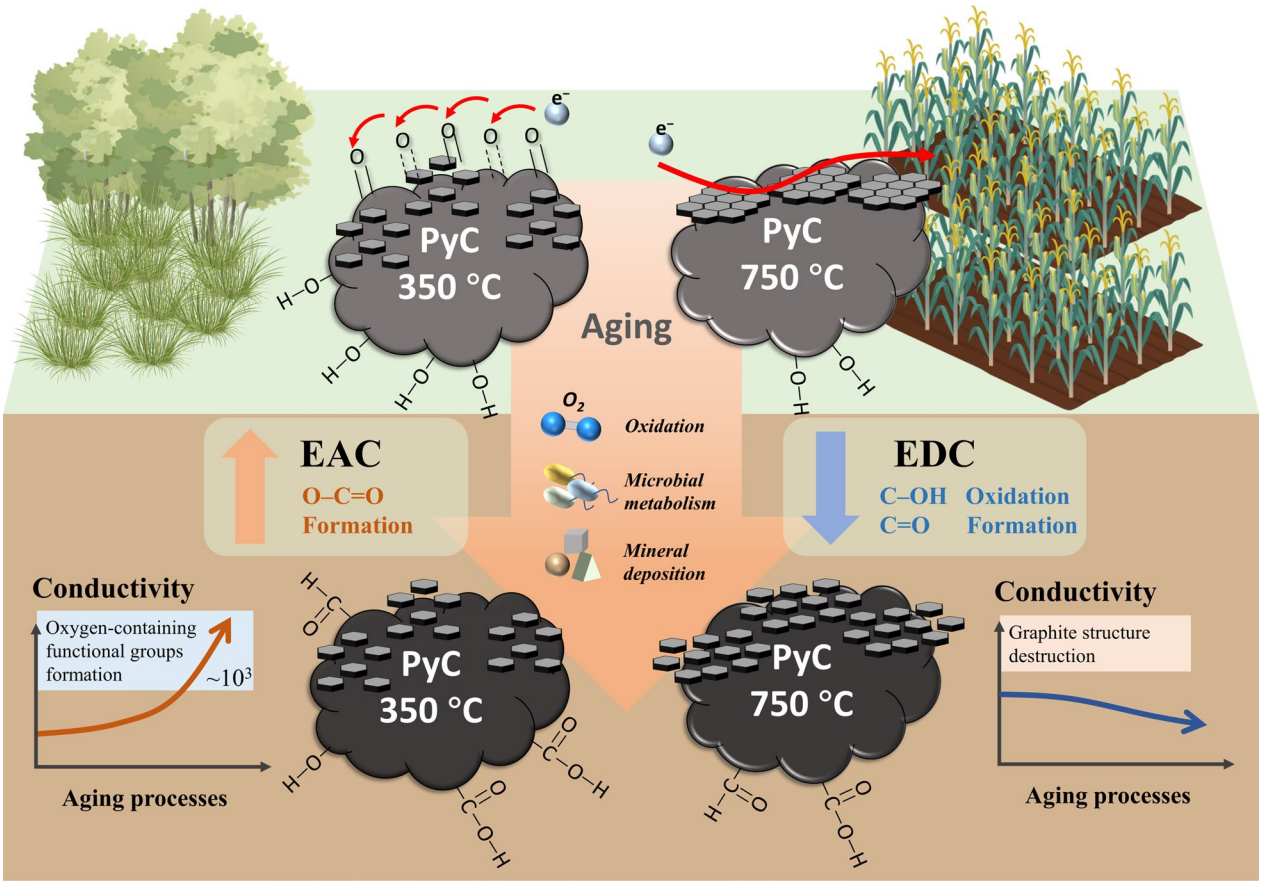

1 Introduction

Pyrogenic carbon (PyC) is a porous, carbon-rich solid material formed through incomplete pyrolysis of organic matter during natural or anthropogenic fires (Kuhlbusch and Crutzen 1995; Santín et al. 2016). It is widespread in both aquatic and terrestrial environments, manifesting as charcoal, biochar, and black carbon (Schmidt and Noack 2000; Si et al. 2023). PyC, a significant component of natural organic matter (Saha et al. 2019; Schievano et al. 2019), constitutes over 30% of total organic carbon in surface soil (Bird et al. 2015; Reisser et al. 2016). Importantly, PyC regulates redox reactions that drive key geochemical and biochemical transformations in aquatic and terrestrial systems, impacting processes such as carbon and nitrogen cycling (Sun et al. 2017), mineral transformations (He et al. 2019; Kappler et al. 2014), and the transformation of organic pollutants (Li et al. 2019; Xu et al. 2016, 2013).

PyC participates in the redox reactions in the biogeochemical cycles based on its electron transfer and exchange properties. The electron transfer properties of PyC are based on the conductive structures of PyC such as condensed polyaromatic carbon matrices, and can be reflected by its conductivity (Xu et al. 2013). Similarly, the electron exchange properties of PyC (i.e., the accepting/donating of electrons) typically occur through the redox moieties of PyC (e.g., quinone/hydroquinone) (Klüpfel et al. 2014), and are typically assessed through the mediated electrochemical approach (Chacón et al. 2017; Prado et al. 2019). Pyrolysis temperature is a key factor affecting the electron transfer capacity of PyC. Generally, the aromaticity/graphitization and specific surface area increase while the aliphaticity and oxygen contents decrease with increasing pyrolysis temperature. At low pyrolysis temperatures, redox-active functional groups mainly contribute to the electron transfer and exchange capacities for the PyC. At high pyrolysis temperature, PyC obtained by carbonization has better crystallinity and conductivity, and the electron transfer through

carbon matrices becomes dominant (Chacón et al. 2017; Mohan et al. 2007; Yuan et al. 2022, 2017). PyC derived from different feedstocks, such as lignin and cellulose, was discovered to exhibit different physicochemical characteristics and electron transfer and exchange properties (Klüpfel et al. 2014).

PyC exhibits long-term stability in the natural environment, with retention times reaching up to 1000 years (Baker et al. 2011). Once entering into the soil, PyC undergoes aging processes that modify its physicochemical properties, including specific surface area and surface functional groups (Mia et al. 2017; Quan et al. 2020). For example, aging could lead to the formation of more acidic functional groups on its surface (e.g., carboxyl and carbonyl groups) (Chang et al. 2019; Wang et al. 2019). The aging of PyC has been extensively studied, with a focus on the physicochemical properties and pollutant adsorption characteristics of PyCs (Tan et al. 2020; Zhao et al. 2015). These studies have demonstrated the significant impact of aging on the core functions of PyC. However, the variation patterns of the electrochemical properties, such as electron transfer and exchange abilities, during the aging process remain unexplored. This research gap limits the comprehensive understanding of the environmental behavior of PyC, necessitating systematic investigation.

In this study, PyC samples derived from four feedstocks and prepared at two pyrolysis temperatures were subjected to three aging methods: chemical aging, freeze–thaw cycling, and natural aging (one year). Chemical aging, an artificial accelerated aging method employed to mimic natural aging processes, was used to significantly reduce observation times and simulate the effects of long-term environmental exposure (Zhao et al. 2023). Additionally, PyC aging can occur due to freeze–thaw events in seasonally frozen areas. The study accelerated these processes by employing an artificial freeze–thaw cycling aging method (Gao et al. 2021). Natural aging (one year) was also included to analyze the combined influence of multiple environmental factors on aging processes (Dong et al. 2017; Wang et al. 2021). The transformation of physical and chemical properties can influence electron transfer and exchange processes. We propose that aging modifies the electron transfer and exchange properties of PyC by introducing redox-active functional groups and by restructuring the polyaromatic carbon structure. This study aims to comprehensively elucidate the effects of aging processes on the electron transfer and exchange properties of PyC. A thorough understanding of these changes is crucial for evaluating the role of PyC in biogeochemical processes.

2 Materials and methods

2.1 Preparation of PyC

In this experiment, four biomass feedstocks were utilized: wood chips (W), straw (S), lignin (L), and cellulose (C). Wood chips (W) was sourced from pine wood, representing a common woody biomass known for its high lignin content. Straw (S) was obtained from rice straw, representing a typical biomass derived from herbaceous plants. Wood chips and straw represented composite biomass, while lignin and cellulose represented pure components of biomass. The biomass feedstock was pyrolyzed in a muffle furnace (SX-4-10, China) under continuous N_2 flow, with a heating rate of 10 °C/min and a residence time of 2 h. According to a previous study, the electron transfer through PyCs produced at pyrolysis temperatures below 400 °C and above 700 °C was based on functional groups and carbon matrices, respectively (Sun et al. 2018). Therefore, the pyrolysis temperatures in this study were set at 350 °C and 750 °C. Following pyrolysis, the PyC samples were directly sieved through a 180-mesh sieve for further use. The PyC samples were designated as X350 or X750, where X represents the feedstock of PyC. PyC samples before aging were denoted as BA.

2.2 Aging processes of PyC

During the chemical aging process, PyC samples were mixed with a 15% H_2O_2 solution at a ratio of 1:20 (mass to volume) and placed in 50 mL centrifuge tubes. The mixture was then continuously agitated in a shaker at 25 °C for 12 h (Tan et al. 2020; Wu et al. 2019; Zhao et al. 2023). Following chemical aging, the PyC samples were rinsed with ultrapure water and subsequently dried in an oven at 105 °C. All chemically aged samples were designated with the prefix "CA".

During freeze–thaw aging, PyC samples were mixed with purified water at a ratio of 1:20 (mass to volume) and placed in 50 mL centrifuge tubes. After agitation at 160 rpm for 2 h, the samples underwent freeze–thaw cycles: initially, the centrifuge tubes were placed in a laboratory refrigerator at − 49 °C for 6 h and then transferred to a constant temperature environment for 18 h (Gao et al. 2021; Hale et al. 2011; Zhang et al. 2019). After experiencing 30 such cycles, the PyC samples were dried in an oven. All samples following freeze–thaw aging were designated with the prefix "FA".

During the natural aging process, soil samples obtained from Kunming, China underwent pretreatment involving drying, grinding, and sieving through a standard 10-mesh sieve to remove large gravel particles, residual roots, and crushed stones. PyC samples were fixed using nylon mesh (0.075 mm) and embedded into the soil sample at a depth of 5 cm over one year. Gravimetric irrigation was carried out every five days until soil moisture reached 40%. The

detailed incubation methodology can be found in SI (text S1) (Gámiz et al. 2019; Rechberger et al. 2017). After the experiment was completed, PyC was extracted from the soil sample, washed with ultrapure water, and then dried in an oven at 105 °C. All samples following natural aging were designated with the prefix "NA". In order to ensure uniformity in the washing process during aging, all PyC samples underwent the same treatment. This involved rinsing with ultrapure water and subsequent oven drying at 105 °C. These samples were labeled with the prefix "W".

2.3 Electron transfer and exchange properties of PyC

The conductivity of PyCs was measured using the conductivity tester (ST2722, Suzhou Jingge Electronics, China) with a four-electrode method (see SI text S2) (Miccoli et al. 2015). The conductivity at different temperatures was determined with a heater located at the bottom of the conductivity tester, which was employed to elevate the temperature from 27 °C to 100 °C. After the temperature stabilized, the conductivity tester measured the conductivity at different temperatures.

The electron donating capacities (EDCs) and electron accepting capacities (EACs) of all PyC samples were determined using mediated electrochemical oxidation (MEO) and mediated electrochemical reduction (MER) methods (Aeschbacher et al. 2010; Klüpfel et al. 2014). These measurements were conducted at applied potentials of + 0.61 V and − 0.49 V (vs. Ag/AgCl reference electrode), respectively. Typically, measurements were performed in a three-electrode system comprising a glass carbon cylinder (60 mL) as the working electrode, a platinum wire as the counter electrode, and an Ag/AgCl electrode as the reference electrode. Diquat dibromide monohydrate (DQ) or 2, 2'-azino-bis-(3-ethyl benzothiazoline-6-sulfonate) diammonium salt (ABTS, > 98%) was added as an electron transfer mediator into the glass carbon cylinder, which contained a buffer solution (0.1 mol/L KCl, 0.1 mol/L phosphate, pH = 7). Upon reaching equilibrium current at a fixed potential, the addition of PyC suspensions (5 g/L) induced significant oxidation and reduction peaks. The EDCs and EACs of PyC samples were calculated by integrating the subsequently generated current peak values using the equations below:

$$EDC = \frac{\int I_{MEO} dt}{F \cdot m_{PyC}} \quad (1)$$

$$EAC = \frac{\int I_{MER} dt}{F \cdot m_{PyC}} \quad (2)$$

I_{MEO} is the current generated during oxidation, I_{MER} is the current generated during reduction [A]. F is the Faraday constant [96485 C/mol e^-], t is the time [sec], m_{PyC} is the mass of PyC added to the system [g], and EDC/EAC is in mmol e^-/g.

2.4 Characterization of PyC

The variation of surface functional groups in PyC after the aging process was investigated using X-ray photoelectron spectroscopy (K-Alpha, Thermo Fisher Scientific, USA) and Fourier transform infrared spectroscopy (Nicolet iS50, Thermo Fisher Scientific, USA). The peak assignments of the XPS and FTIR spectra are shown in Table S1 and S2. The XPS spectra were calibrated according to the C1s peak (284.8 eV), smoothed and peak fitted by XPSPEAK software. The C1s peaks were fitted with sp^2 (284.6 eV), sp^3 (285.2 eV), C–O (286.8 eV), C=O (288.9 eV), and π–π* (291.0 eV) features (Varga et al. 2017). The O1s peaks were fitted with quinone (531.2 eV), C=O (532.5 eV), C–OH (533.7 eV), and –COOH (534.3–535.4 eV) features (Li et al. 2020). The Raman measurement was conducted by Raman spectroscopy (Horiba Jobin Yvon XploRA, HORIBA, France) to characterize the ordered and amorphous carbon. The acquired data were baseline corrected in the wavelength range of 800–2000 cm^{-1}, and the I_D/I_G values were determined by comparing the peak height of the D-peak and the G-peak on the plotted area. Particle size analysis of PyC was conducted using a size analyzer (Mastersizer 2000 particle, Malvern, UK). The specific surface areas of PyC samples were determined using a surface area analyzer (Autosorb IQ, Kantar Instruments, USA). The surface and pore structure of PyC were observed using a scanning electron microscope (Regulus 8230, Hitachi, China).

3 Results and discussion

3.1 Aging-induced reduction of conductivity in PyC at 750 °C attributed to damage of polyaromatic carbon matrices

As the pyrolysis temperature rises, components like lignin and cellulose decompose, forming polyaromatic carbon structures (Klüpfel et al. 2014; Sun et al. 2017). The conductivities of PyC produced at 750 °C ranged from 0.1 to 5.0 S/cm (Fig. 1a), representing a 10^8–10^{11}-fold increase compared to those produced at 350 °C (Fig. 2a). Notably, L750 exhibited the highest conductivity (4.65 S/cm), significantly exceeding other PyC samples (0.43 to 1.53 S/cm). However, aging led to a general conductivity decline in most PyC samples produced at 750 °C. Enhancement rates below one confirmed this conductivity reduction (Fig. 1b). Post-aging analysis revealed that the average conductivities of PyC produced at 750 °C decreased to 0.65, 0.58, and 0.31 times their

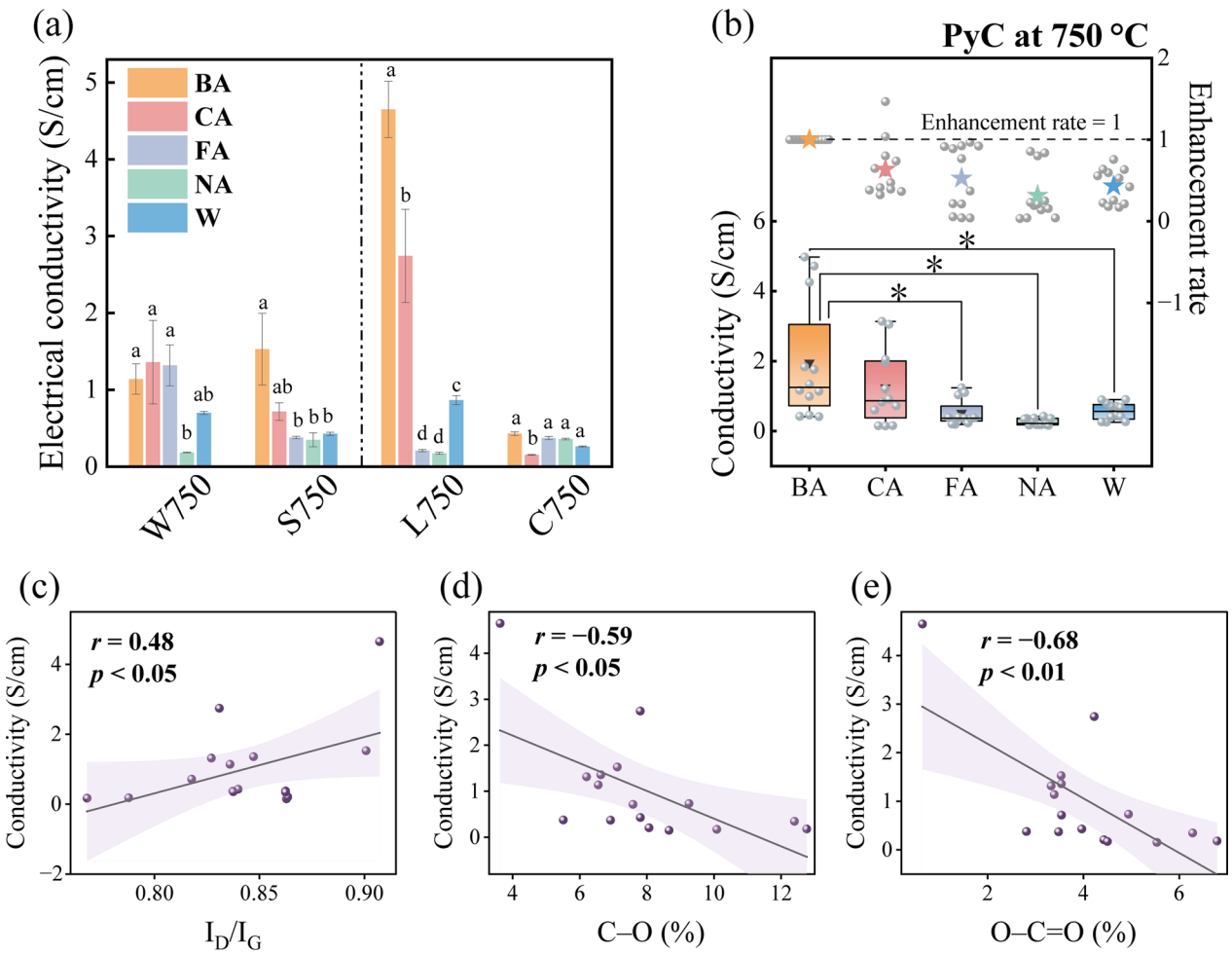

Fig. 1 The conductivity of pyrogenic carbon (PyC) produced at 750 °C (**a**). Comprehensive analysis of conductivity variation induced by aging (**b**). Linear relationships between conductivity and I_D/I_G ratio (**c**), C–O content (**d**), and O–C=O content (**e**). The PyC samples were designated as X750, where X represents the feedstock of PyC: wood chips (W), straw (S), lignin (L), and cellulose (C). Five treatments were applied: before aging (BA), chemical aging (CA), freeze–thaw aging (FA), natural aging (NA), water washing (W)

original values after chemical aging, freeze–thaw aging, and natural aging, respectively (Fig. 1b).

The conductivity of PyC produced at 750 °C showed a significant positive correlation with the I_D/I_G ratio (Fig. 1c, $p < 0.05$). Higher I_D/I_G values reflect greater structural ordering in PyC's polyaromatic carbon matrices, enabling more efficient electron transfer pathways and thus enhancing conductivity (Sun et al. 2017). Previous research has demonstrated that feedstocks with higher lignin content promote the formation of these well-ordered polyaromatic structures in PyC (Wang et al. 2020). Accordingly, L750 exhibited the highest conductivity (4.65 S/cm) prior to aging (Fig. 1a). Aging reduced the I_D/I_G ratios by 3.39% (CA) and 6.42% (NA) (Fig. S1), damaging the polyaromatic carbon matrices and leading to the decline in conductivity. Furthermore, negative correlations were observed between conductivity and oxygen-containing functional groups (C–O and O–C=O groups) (Fig. 1d and e). The aging process driven by biotic and abiotic oxidation increased the abundance of these oxygen-containing functional groups, which impeded electron transfer through the carbon matrices (Fan et al. 2018). Water washing also reduced the conductivity of PyC produced at 750 °C to 43% of its initial value (Fig. 1b). The mean I_D/I_G ratio decreased to 0.91 times its original value after water washing (Fig. S1e), further supporting the conclusion that water washing can disrupt the polyaromatic carbon structure of PyC produced at 750 °C (Çetin et al. 2013). However, no significant difference in I_D/I_G ratio was observed between NA and W (Fig. S33), indicating that in addition to polyaromatic carbon structural changes, microbial degradation and abiotic oxidation during natural aging also contribute to electrical conductivity reduction. These processes increase

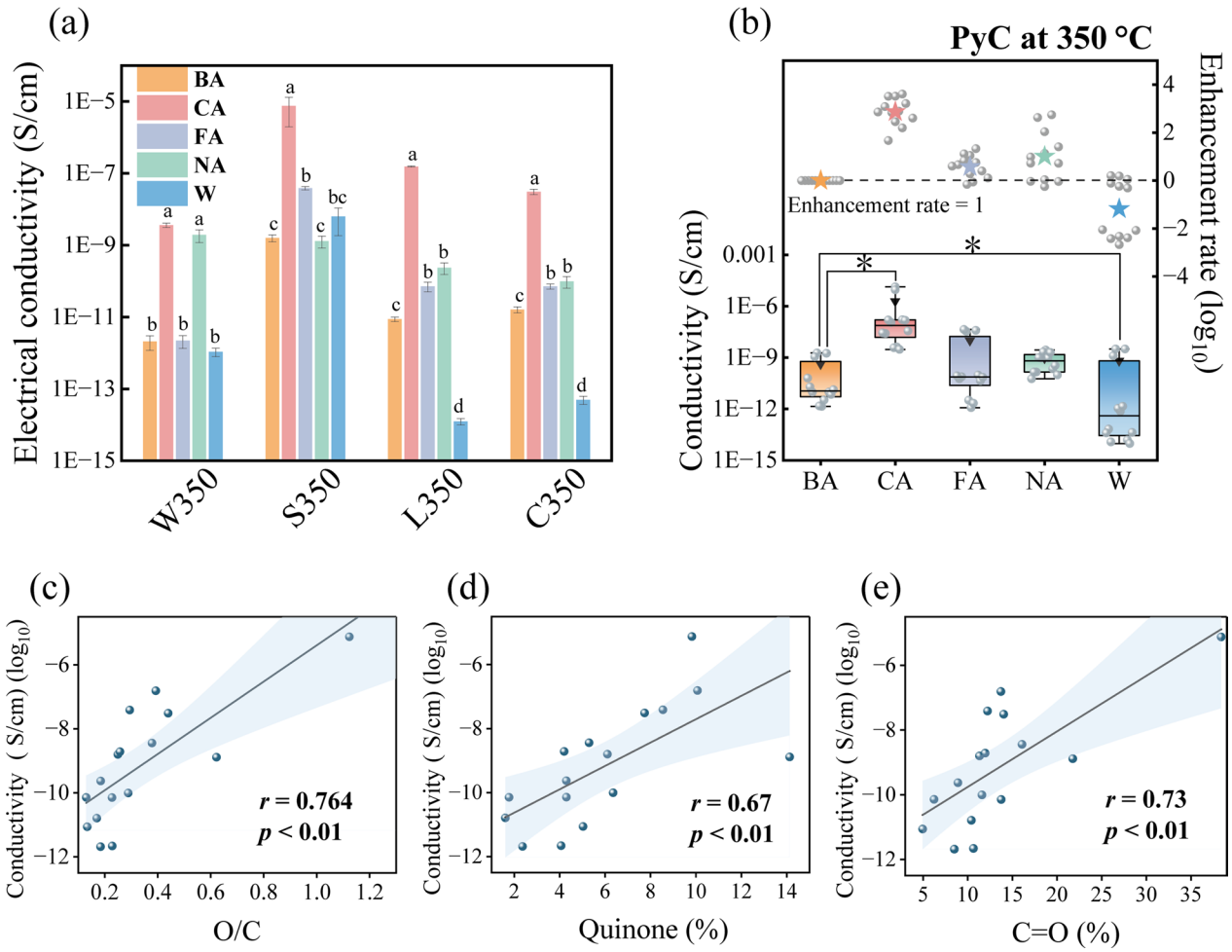

Fig. 2 The conductivity of PyC produced at 350 °C (**a**). Comprehensive analysis of conductivity variation induced by aging (**b**). Linear relationships between conductivity and O/C ratio (**c**), quinone content (**d**), and C=O content (**e**)

oxygen-containing functional groups (e.g., C–O and O–C=O) that impede electron transfer (Rechberger et al. 2017). Furthermore, certain oxygen-containing functional groups that may enhance conductivity are hydrophilic and could be lost during water washing.

3.2 Aging-induced increase in conductivity of PyC produced at 350 °C attributed to the enrichment of redox-active functional groups

As shown in Fig. 2a, the conductivities of PyC produced at 350 °C remained consistently below 1×10^{-8} S/m. At this temperature, PyC primarily consists of aliphatic carbon, which exhibits limited electron transfer capability (Ameloot et al. 2013). Sample S350 demonstrated a conductivity of 1.59×10^{-9} S/cm, significantly higher than that of the other three samples (2.08×10^{-12} to 1.62×10^{-11} S/cm). An enhancement rate greater than one indicated that aging positively influenced PyC conductivity. As evidenced in Fig. 2b, most enhancement rates exceeded one, confirming that aging increased the conductivity of PyC produced at 350 °C. The average enhancement rates followed this descending order: CA, NA, and FA (Fig. 2b). Specifically, aging increased the conductivity of PyC produced at 350 °C by factors of 6539.75 (CA), 240.44 (NA), and 9.53 (FA), corresponding to logarithmic values of 3.61, 1.27, and 0.74, respectively. These results demonstrate that aging significantly improves the conductivity of PyC produced at 350 °C, with chemical aging exhibiting the most pronounced effect.

A significant positive correlation was observed between the conductivities of PyC produced at 350 °C and their O/C ratios ($p<0.01$), as depicted in Fig. 2c. This correlation suggests that the increased conductivity of PyC produced at 350 °C after aging can be attributed to the formation of additional oxygen-containing functional groups. Notably, PyC sample S350, with the highest O content (24.97%, Fig. S10a), showed the highest

conductivity among the four PyC samples produced at 350 °C. Further analysis, shown in Fig. S10c, indicated that all aging processes led to an increase in the O/C ratio for PyC produced at 350 °C. Among these processes, chemical aging exhibited the most significant promotion effect on the O/C ratio, with an average enhancement rate of 3.02 times, surpassing the enhancement rates observed for freeze–thaw aging and natural aging, which had average enhancement rates of 1.18 and 1.74 times, respectively.

The study revealed a significant positive correlation between the conductivities of PyC produced at 350 °C and the content of quinone and carbonyl (–C=O) groups (Fig. 1d and 1e). The average quinone content increased by 2.67, 1.27, and 2.22 times the original PyC content following chemical aging, freeze–thaw aging, and natural aging, respectively (Fig. S19). Similarly, the average carbonyl (–C=O) group content increased by 2.35, 1.23, and 1.56 times the original PyC content after chemical aging, freeze–thaw aging, and natural aging, respectively (Fig. S28). The oxidation induced by H_2O_2 during chemical aging and microbial oxidation activities during natural aging resulted in a significant rise in oxygen-containing functional groups like quinones and carbonyls on the PyC surface (Liu and Fan 2022; Saeed et al. 2019). One-year natural aging reveals early-stage aging mechanisms where rapid surface oxidation precedes structural changes (Dong et al. 2017). These observations underscore the importance of oxygen-containing functional groups, particularly quinones and carbonyls, in enhancing the electrical conductivity of PyC. Furthermore, all three aging processes involved a hydro-washing effect to some extent, which reduced the conductivity of PyC produced at 350 °C (Fig. 1b). This suggests that the conductivity improvement from aging at 350 °C primarily stems from the increase in oxygen-containing functional groups rather than hydrodynamic washing effects.

It has been consistently emphasized that PyC contains redox-active functional groups and polyaromatic carbon matrices, both of which facilitate electron transfer (Sun et al. 2018). In this study, we demonstrated that the conductivity of PyC produced at 350 °C is mainly driven by electron transfer processes involving "redox-active moieties", specifically oxygen-containing functional groups, rather than conductive polyaromatic carbon matrices (Dasgupta et al. 1991; Fan et al. 2018). This was supported by the mechanism wherein *p* orbitals on oxygen-containing functional groups such as the –C=O group can create a conjugated structure through superposition, enabling electron transfer via alternating single and double bonds (Jackson et al. 2013; Saha et al. 2019). Compared to polyaromatic carbon matrices, the electron transfer process through redox-active functional groups is more influenced by molecular thermal motion (Eckert et al. 1988; Helmbold et al. 1995). As the testing temperature increased from 27 °C to 100 °C, the conductivity of PyC produced at 350 °C significantly increased (Fig. 3a). In contrast, the conductivity of PyC produced at 750 °C remained constant. This test further confirmed that the conductivities of PyC produced at 350 °C and 750 °C primarily depend on oxygen-containing functional groups and polyaromatic carbon matrices, respectively.

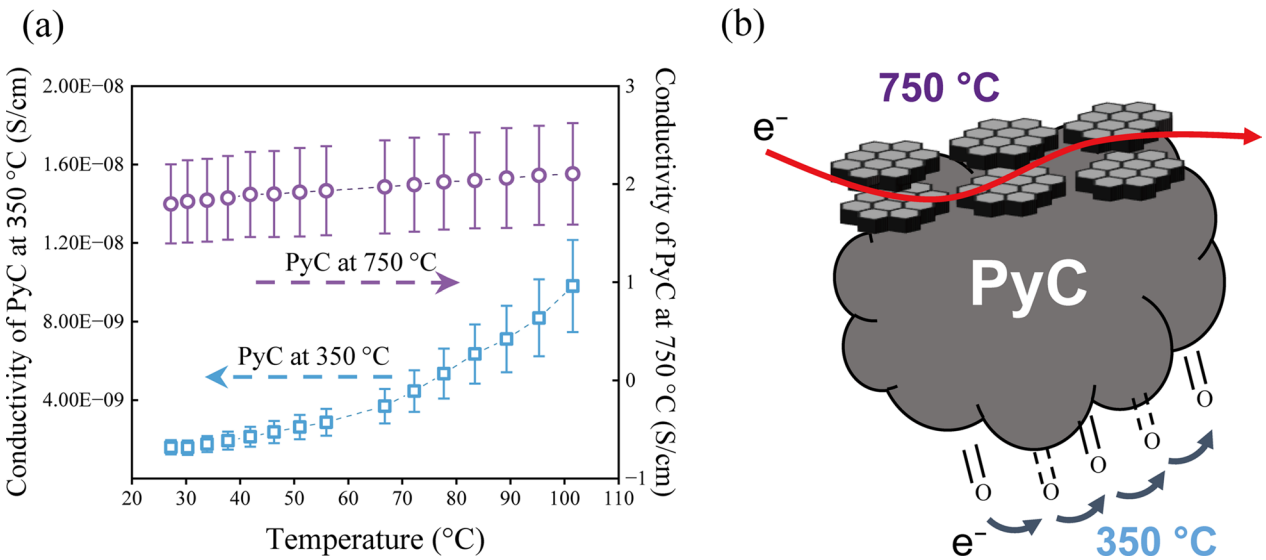

Fig. 3 The conductivity variation of pyrogenic carbon at different temperatures (**a**). Schematic diagram of the electron transfer mechanisms of pyrogenic carbon produced at 350 °C and 750 °C (**b**)

Conductivity of PyC produced at 350 °C is predominantly governed by redox-active functional groups, a common feature observed in various polymer materials (Akhoury et al. 2013). A filament characterized by π-stacking of aromatic side chains, exhibits a conductivity of approximately 1×10^{-6} S/cm (Gu et al. 2021). Cryo-EM analysis of the filament structure showed an average distance of 10 Å between aromatic residues. As electron transfer efficiency decreases with greater distances, the lower conductivity of PyC produced at 350 °C compared to the filament implied that the separations between redox-active functional groups in PyC produced at this temperature exceed 10 Å. Previous studies on PyC conductivity primarily have emphasized the polyaromatic carbon matrices as the foundational framework for electron transfer (Sun et al. 2017). Our investigation demonstrates that redox moieties, including oxygen-containing functional groups, may also play a role in electron transfer in PyC produced at relatively low pyrolysis temperatures.

3.3 Aging effects on EDC of PyC

As shown in Fig. 4a, the EDCs of PyC produced at 350 °C ranged from 0.05 to 0.35 mmol e^-/g prior to aging. Specifically, PyC derived from lignin (L350) exhibited an EDC of 0.19 ± 0.05 mmol e^-/g, which was higher than that of PyC derived from cellulose (C350, 0.05 ± 0.01 mmol e^-/g). Consequently, the EDC of W350 (0.35 ± 0.09 mmol e^-/g), primarily sourced from lignin, exceeded that of S350 (0.15 ± 0.05 mmol e^-/g). After aging, most EDCs of PyC produced at 350 °C exhibited a decreasing trend (Fig. 4b). On average, EDCs were reduced to approximately 0.48 and 0.5 times their original values after freeze–thaw aging and natural aging, respectively. In contrast, the EDC of C350 significantly increased from 0.05 ± 0.007 mmol e^-/g (BA) to 0.19 ± 0.035 mmol e^-/g and 0.07 ± 0.01 mmol e^-/g after chemical aging and natural aging, respectively (Fig. 4a).

As illustrated in Fig. 4c, the EDC of PyC produced at 350 °C demonstrated a significant positive correlation with the C–OH content ($p<0.01$), known for its electron donating ability (Prévoteau et al. 2016; Saquing et al. 2016). Aging processes typically convert the C–OH groups in PyC to higher oxidation state groups like carbonyl (C=O) and carboxyl (O–C=O) groups (Nie et al. 2019). As shown in Fig. S29, except for C350, the average C–OH contents of PyC produced at 350 °C decreased to 0.74 and 0.67 times of the original levels after chemical aging and natural aging, respectively. Conversely, the C–OH content of C350 increased by factors of 1.20 and 1.12 after chemical aging and natural aging, respectively (Fig. S29). Furthermore, FTIR analysis revealed that chemical aging significantly increased the peak areas associated with C–OH groups in C350 (Fig. S30). This distinct behavior can be attributed to the unique composition of cellulose, a polymer comprising glucose molecules linked by β-1,4-glycosidic bonds (Costantini et al. 2020). During PyC aging, cleavage of these glucose units generated products with elevated phenolic group content (Wang et al. 2023), which contributed to the observed increase in EDC for aged C350 samples.

At 750 °C, L750 showed the highest EDC value of 0.14 ± 0.01 mmol e^-/g, while other PyC samples displayed EDCs ranging from 0.02 to 0.08 mmol e^-/g (Fig. 4a). FTIR analysis revealed that most surface functional groups of PyC samples had decomposed at 750 °C, leaving trace amounts of ether (1110 cm^{-1}) and phenol groups (3200–3500 cm^{-1}) (Fig. S30). The phenol peak area of L750 was the most prominent among the PyC samples, contributing to its highest EDC value (Fig. 4a). A significant negative correlation was observed between PyC EDCs and C=O content, as C–OH groups on the surface were converted to C=O upon aging, leading to reduced EDC levels (Chang et al. 2019; Wang et al. 2019). However, the EDCs of PyC produced at 750 °C did not consistently decrease after aging (Fig. 4d), suggesting the involvement of other influencing factors. The content of electron-donating functional groups like C–OH was significantly lower in PyC produced at 750 °C than in PyC produced at 350 °C. Additionally, the physical and chemical characteristics of PyC produced at 750 °C varied depending on the type of feedstock. Our results indicate that PyC derived from cellulose-rich biomass (S750 and C750) consistently exhibited enhanced EDC after chemical aging and natural aging treatments. This phenomenon is attributed to the unique polymer structure of cellulose, which offers superior microbial accessibility compared to lignin. As a result, PyCs derived from cellulose decompose rapidly during aging processes, leading to the generation of phenolic oxidation products that boost EDC (Lyu et al. 2021; Wang et al. 2023). These feedstock-specific aging patterns have significant environmental implications for long-term applications. Cellulose-derived PyC's ability to enhance EDC suggests a potential to stimulate microbial metabolic processes by providing sustained electron donation, while PyC derived from lignin is expected to exhibit more stable behavior.

3.4 Aging effects on EAC of PyC

The EAC of PyC produced at 350 °C was relatively low, ranging from 0.04 to 0.05 mmol e^-/g (Fig. 5a). However, chemical aging significantly increased the EACs of PyC produced at 350 °C, with an average enhancement rate of 3.41. In contrast, natural aging reduced the EACs of all PyC produced at 350 °C to an average of 3.65% of their original values (Fig. 5b). A strong positive

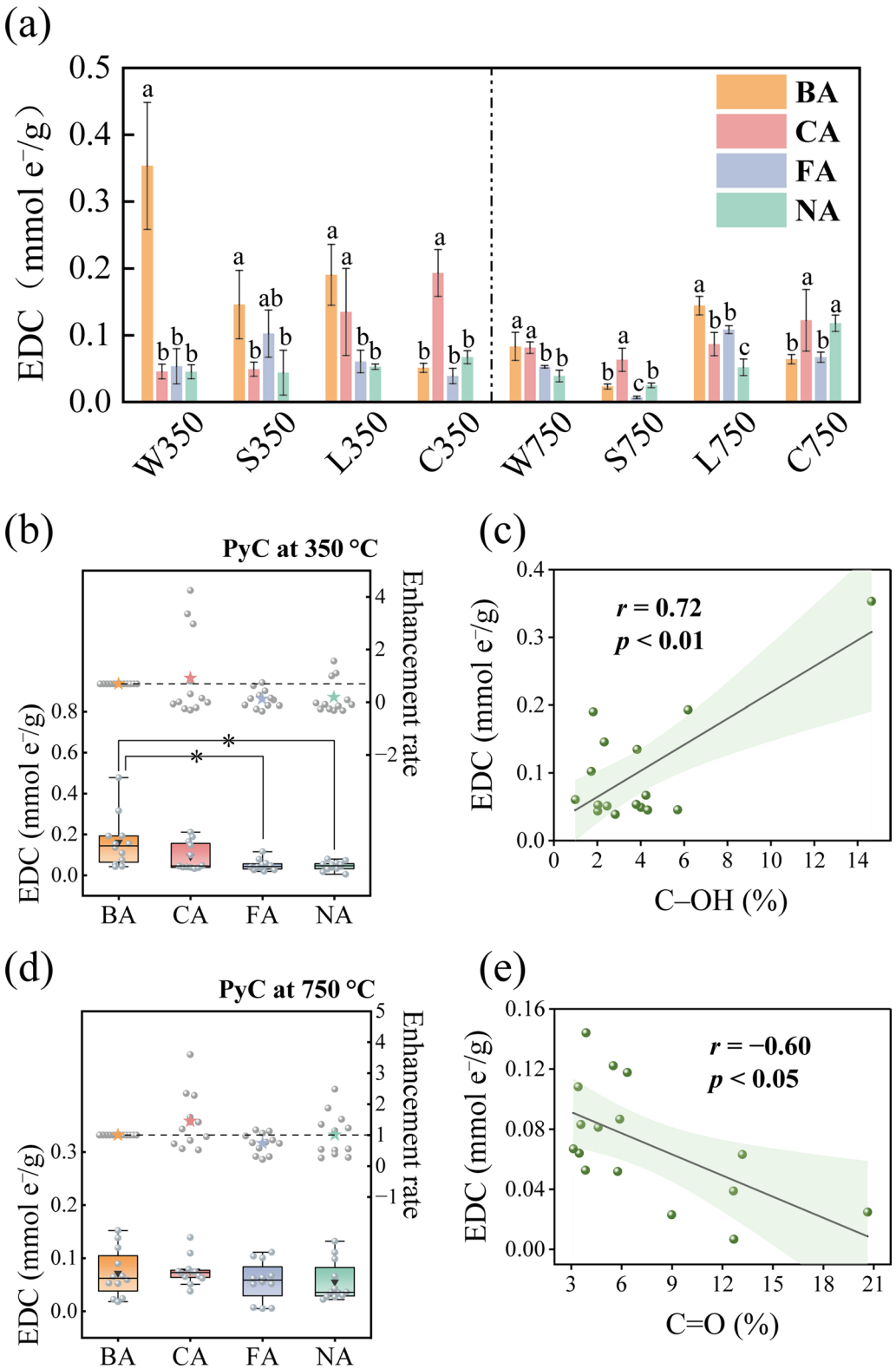

Fig. 4 The electron donating capacities (EDCs) of PyC before and after aging (**a**). Comprehensive analysis of EDC variation of PyC produced at 350 °C due to aging (**b**). Linear relationship between EDCs and the content of C–OH (**c**). Comprehensive analysis of EDC variation of PyC produced at 750 °C due to aging (**d**). Linear relationship between EDCs and the content of C=O (**e**)

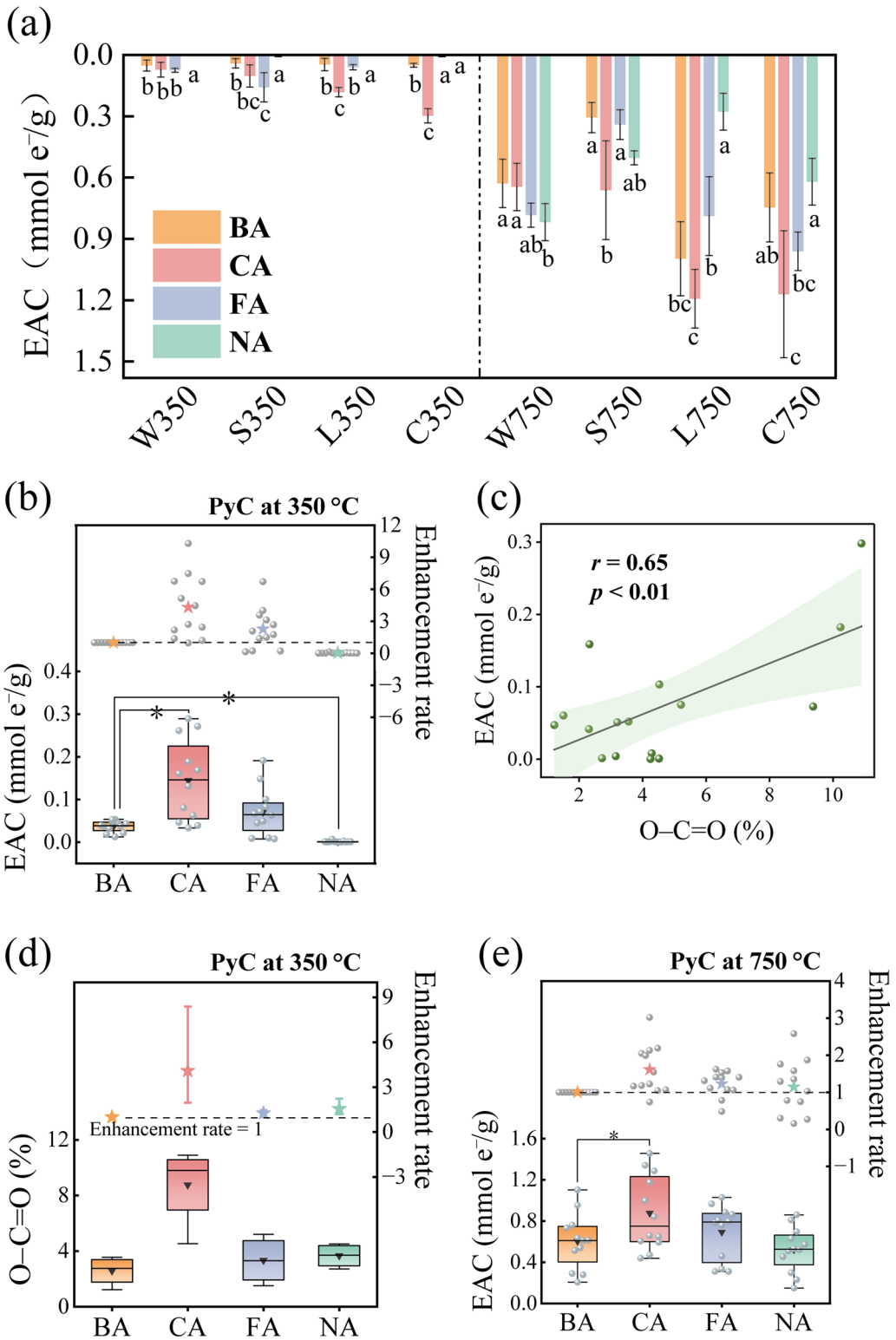

Fig. 5 The electron accepting capacities (EACs) of PyC before and after aging (**a**). Comprehensive analysis of EACs of PyC produced at 350 °C (**b**). Linear relationship between EACs and the content of O–C=O (**c**). Comprehensive analysis of the O–C=O content of PyC produced at 750 °C (**d**). Comprehensive analysis of EACs of PyC produced at 750 °C (**e**)

correlation was observed between EAC and the content of O–C=O ($p < 0.01$, Fig. 5c), attributed to their electron-accepting capability (Saha et al. 2019). FTIR analysis (Fig. S30) revealed the formation of a new –COOH peak (1692 cm^{-1}) in PyC produced at 350 °C after chemical aging, indicating rapid oxidation of phenolic hydroxyl groups to electron-accepting carboxyl groups. Additionally, chemical aging increased the specific surface area of PyC by 22.57-fold compared to that of the before aging samples (Fig. S31). This expansion in surface area likely exposed more redox-active moieties, further enhancing electron acceptance. Collectively, these findings demonstrated that chemical aging substantially improves the electron-accepting properties of PyC produced at 350 °C by increasing both the abundance and accessibility of electron-accepting functional groups.

Following natural aging, the –COOH content of PyC produced at 350 °C increased by 1.74 times compared to pre-aging levels, yet the EAC decreased consistently. Natural aging resulted in the enrichment of minerals on all PyC surfaces, notably with a significant increase in Si content to 4.46% (Fig. S32). Moreover, an increase in Ca content was observed in W350, S350, and C350 samples. Previous studies have suggested that minerals can create organometallic complexes on the PyC surface during natural aging, leading to a reduction in EAC (Wang et al. 2021; Yang et al. 2016). This phenomenon suggests that long-term PyC application may mitigate greenhouse gas (CO_2/CH_4/N_2O) emissions through the physical coverage of electrochemically active surfaces by mineral coatings. The I_D/I_G values of PyCs produced at 350 °C were apparently lower than those of BA (Fig. S33), indicating a lower condensed carbon content, which is crucial for the redox properties of PyC as an electron acceptor (Li et al. 2020). The decrease in condensed carbon content after natural aging primarily contributed to the decline in EAC. Therefore, while natural aging increases certain electron-accepting functional groups such as –COOH, the formation of organometallic complexes and the reduction in condensed carbon content significantly diminish the EAC of PyC. Chemical aging is commonly employed to expedite the aging process and replicate natural aging procedures (Zhao et al. 2023). When considering the electron transfer and exchange characteristics of PyC, the changes induced by chemical aging closely resemble those seen with natural aging. Nevertheless, the alterations in EACs resulting from chemical aging and natural aging exhibit divergent patterns. This discovery suggests that substituting chemical aging for natural aging in investigations of EAC-related geochemical phenomena may yield erroneous results.

As illustrated in Fig. 5a, the EACs of PyC produced at 750 °C ranged from 0.63 to 1.00 mmol e^-/g, representing a 6.40- to 20.17-fold increase compared to PyC produced at 350 °C. Increasing the pyrolysis temperatures resulted in graphitization, which enhanced the effective surface area of the carbon material. This enhancement is supported by the data presented in Fig. S33, showing that the I_D/I_G ratios for PyC produced at 350 °C ranged from 0.67 to 0.72, whereas for PyC produced at 750 °C, they ranged from 0.84 to 0.91. Chemical aging significantly boosted the EAC of PyC produced at 750 °C, increasing its average value by 1.49 times compared to its original value. This enhancement was attributed to the elevated content of O–C=O groups, which increased by 68% after chemical aging (Fig. S34). These groups are capable of donating more electrons than other groups. However, freezing and thawing and natural aging exhibited inconsistent effects on the EAC of PyC produced at 750 °C (Fig. 5e), indicating that multiple moieties and structural properties were involved in the EAC of PyC. For instance, while chemical aging enhances EAC by increasing electron-donating functional groups, freeze–thaw aging and natural aging may introduce changes that either positively or negatively impact the EAC, such as alterations in physical structure or the formation of new functional groups. PyC can function as an electron shuttle to facilitate the reduction of ferrihydrite by Fe(III) mineral-reducing bacteria (Kappler et al. 2014). Our results suggest that the decrease in PyC's EDC due to aging could impede electron transfer between microbes and Fe(III) minerals, potentially limiting direct redox reactions with metal ions. Furthermore, PyC has been observed to act as an electron acceptor, enhancing intracellular electron transfer in denitrifying anaerobic methane-oxidizing (DAMO) archaea, thereby directing more electrons towards the membrane for nitrate reduction (Lv et al. 2024). The aging-induced increase in EAC of PyC may further enhance these effects.

3.5 Implications of aging-induced electron transfer and exchange properties changes in PyC

Our findings reveal that aging induces a fundamental shift in the electron exchange properties of PyC, characterized by enhanced EAC, and reduced EDC. This transformation to a state more inclined to accept electrons but less willing to donate them has significant implications for its role in agricultural and environmental systems (Fig. 6). In agriculture, this evolution offers a combination of synergistic benefits and potential trade-offs. Aged PyC, with enhanced EAC, can improve nitrogen cycling by promoting ammonium oxidation to nitrate, potentially increasing crop nitrogen use efficiency (Wang et al. 2015). Furthermore, its increased electron affinity aids in retaining cationic nutrients like potassium and calcium, reducing their leaching (Wu et al. 2025). A moderately

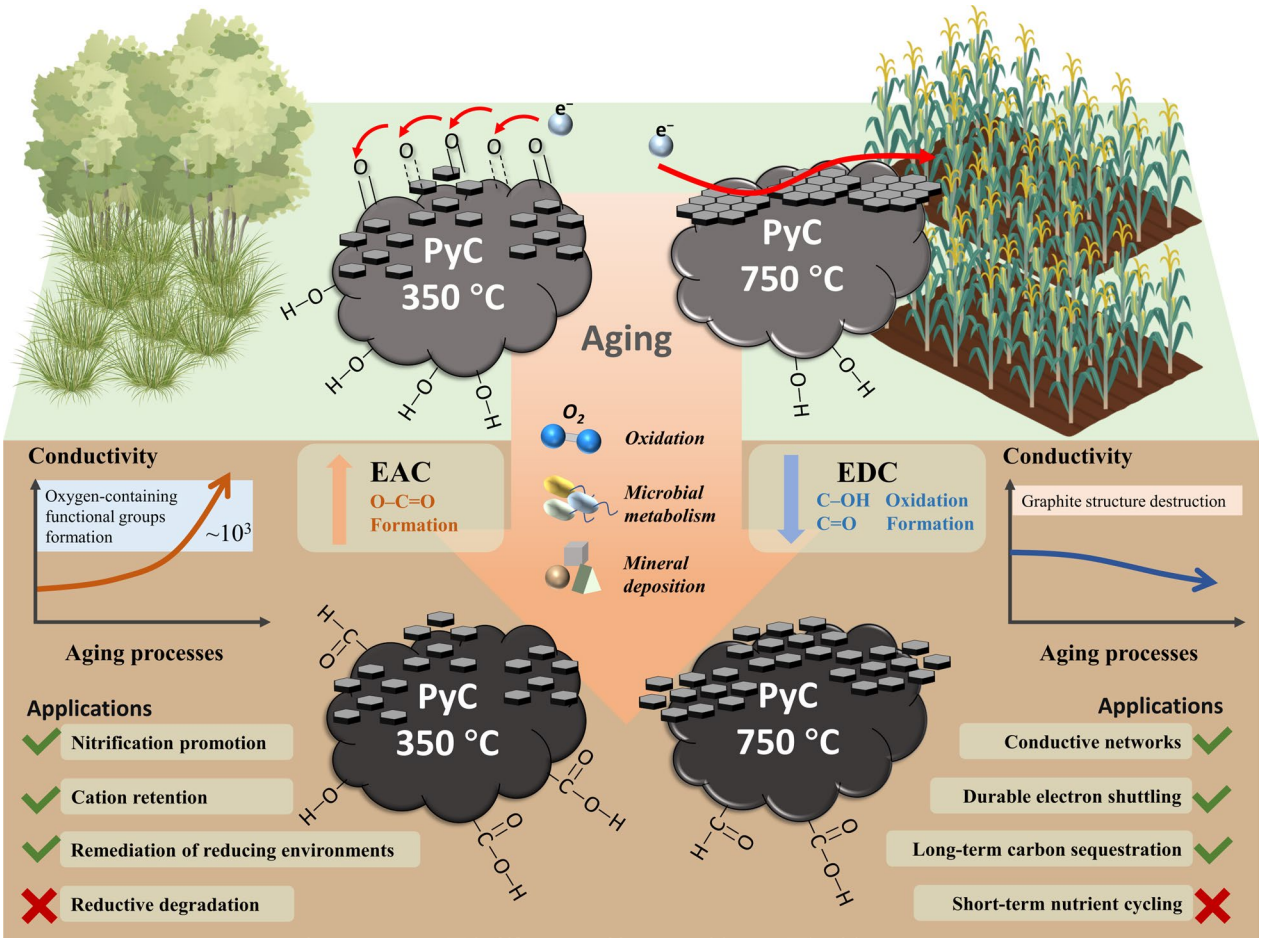

Fig. 6 Potential environmental impacts due to aging-induced changes in electrochemical properties of PyC

elevated oxidation–reduction potential may also foster aerobic microorganisms while suppressing anaerobic pathogens. However, these advantages require careful management to avoid risks. Excessive nitrification might cause nitrate leaching, posing an environmental threat. The more oxidized nature of aged PyC could undermine the soil acidification mitigation of fresh biochar and, in extreme cases, induce oxidative stress in plants or inhibit beneficial anaerobic microbial communities. Regarding heavy metals, the aging of PyC, characterized by increased EAC, can enhance the adsorption of cationic species and facilitate the reductive immobilization of toxic Cr(VI) (Shang et al. 2024; Wu et al. 2025). Nevertheless, the loss of EDC eventually diminishes the material's reducing capacity, risking the re-mobilization of previously immobilized metals. Thus, the effectiveness of aged PyC is highly dependent on environmental conditions: it is promising for remediating strongly reducing environments by consuming excess electrons but likely ineffective in highly oxidizing settings.

Biochar and activated carbon, widely used in environmental or technological applications, are forms of pyrogenic carbon. Their electrochemical properties undergo analogous changes after aging. High-temperature biochar and activated carbon exhibit a significant decrease in conductivity after aging, while low-temperature biochar may experience an increase. However, regarding electron exchange capacities, high-temperature biochar and activated carbon show no consistent trends after aging. In contrast, low-temperature biochar exhibits a decrease in EDC and an increase in EAC after aging, due to the oxidation of these materials during the aging process.

The strategic application of PyC must be guided by its production temperature and the specific redox requirements of the target environment, while also considering the aging-induced changes in PyC properties. Distinct aging pathways further differentiate their long-term functionality: the conductivity of low-temperature PyC shows an increase after aging, which may enhance its role in short-term electron transfer processes, while the conductivity of high-temperature PyC experiences

a decrease, though it maintains a high level suitable for persistent electron shuttling. Considering these changes, low-temperature PyC, with its higher bioavailability and more labile carbon pools, remains suitable for short-term interventions aimed at enhancing nutrient cycling and treating anaerobic contamination. In contrast, the persistent conductivity and stability of high-temperature PyC recommend it for long-term carbon sequestration strategies and applications requiring durable electron-shuttling capabilities. Ultimately, our results underscore the necessity of a precision-based approach, potentially involving tailored blends of PyC, to harness these contrasting properties for synergistic outcomes that address both immediate functional goals and long-term stability in agricultural and environmental management.

4 Conclusion

PyC exists in various forms across atmospheric, terrestrial, and aquatic systems, such as soils, sediments, ice, and marine environments, ranging from macroscopic fragments to individual molecules. Despite its widespread presence, the environmental impacts of PyC remain inadequately characterized. Our research demonstrates that the electron transfer properties of PyC are modified by aging in varying ways, contingent upon the pyrolysis temperature. We observed inhibitory effects in PyC produced at high temperatures, while PyC generated at low temperatures showed enhancements, which could impact the redox reactions integral to geochemical cycles.

Aged low-temperature PyC produced at 350 °C exhibits an increased EAC, potentially enhancing pollutant degradation in aquatic systems, by facilitating the reduction of oxidized contaminants such as nitroaromatic compounds through abiotic electron transfer processes (Zhao et al. 2021; Zhu et al. 2017). In contrast, high-temperature PyC produced at 750 °C experiences a decrease in conductivity with aging. This characteristic may influence specific microbial respiration pathways, as the preserved yet less conductive carbon matrix could restrict direct interspecies electron transfer between syntrophic microorganisms (Zhao et al. 2016), potentially altering methane production pathways (Sun et al. 2021). These findings suggest that aged high-temperature PyC may selectively regulate microbial communities rather than universally inhibit respiratory processes. The temperature-dependent behaviors of PyC underscore its potential as a modifiable environmental amendment. Therefore, estimating the environmental impact of PyC based on its electron transfer and exchange properties should account for this variation due to aging. These results underscore the importance of considering aging-induced variations in electron transfer and exchange capabilities when evaluating the environmental repercussions of PyC. This insight is crucial for forecasting the long-term environmental behavior of PyC and its involvement in geochemical processes.

Supplementary Information

The online version contains supplementary material available at https://doi.org/10.1007/s42773-025-00546-z.

Additional file 1: Text S1. Nature aging incubation method; Text S2. Conductivity measurement method. Table S1. Assignment of photon energy to C forms in C 1s XPS; Table S2. Assignments of vibration wavenumbers in FTIR to moieties of PyC; Table S3. Aging induced changes in PyC properties. Fig. S1. Comprehensive analysis of ID/IG values changes after PyC aging and water washing at 750 °C; Fig. S2. The full spectrum of W350 XPS; Fig. S3. The full spectrum of S350 XPS; Fig. S4. The full spectrum of L350 XPS; Fig. S5. The full spectrum of C350 XPS; Fig. S6. The full spectrum of W750 XPS; Fig. S7. The full spectrum of S750 XPS; Fig. S8. The full spectrum of L750 XPS; Fig. S9. The full spectrum of C750 XPS; Fig. S10. 350 °C PyC sample the O/C ratio after various aging processes.; Fig. S11. Peak plot of XPS fine spectrum of W350 O1s; Fig. S12. Peak plot of XPS fine spectrum of S350 O1s; Fig. S13. Peak plot of XPS fine spectrum of L350 O1s; Fig. S14. Peak plot of XPS fine spectrum of C350 O1s; Fig. S15. Peak plot of XPS fine spectrum of W750 O1s; Fig. S16. Peak plot of XPS fine spectrum of S750 O1s; Fig. S17. Peak plot of XPS fine spectrum of L750 O1s; Fig. S18. Peak plot of XPS fine spectrum of C750 O1s; Fig. S19. The change value of the quinone content of PyC at 350 °C after aging; Fig. S20. Peak plot of XPS fine spectrum of W350 C1s; Fig. S21. Peak plot of XPS fine spectrum of S350 C1s; Fig. S22. Peak plot of XPS fine spectrum of L350 C1s; Fig. S23. Peak plot of XPS fine spectrum of C350 C1s; Fig. S24. Peak plot of XPS fine spectrum of W750 C1s; Fig. S25. Peak plot of XPS fine spectrum of S750 C1s; Fig. S26. Peak plot of XPS fine spectrum of L750 C1s; Fig. S27. Peak plot of XPS fine spectrum of C750 C1s; Fig. S28. After aging, the carbonyl content (–C=O) changes the value of PyC at 350 °C; Fig. S29. Comprehensive analysis of phenolic group content after different aging processes; Fig. S30. FTIR analysis of pyrogenic carbon; Fig. S31. Comprehensive analysis of the specific surface area of pyrogenic carbon at 350 °C after different aging processes; Fig. S32. Mineral components analysis of pyrogenic carbon; Fig. S33. Raman spectroscopy analysis of pyrogenic carbon; Fig. S34. The comprehensive analysis of O–C=O of pyrogenic carbon at 750 °C after different aging processes.

Author contributions

Mulin Cao: investigation, data analysis, visualization, writing review and editing. Hao Ren: material preparation, investigation, data collection and analysis. Pengxiang Zhu: data collection. Wenmei Tao: review and editing. Wei Du: review and editing. Hao Li: review and editing. Yandi Hu: review and editing. Peng Zhang: conceptualization, supervision, review and editing, funding acquisition. Bo Pan: supervision, review and editing, funding acquisition. All authors read and approved the final manuscript.

Funding

This work was supported by the Yunnan Provincial Science and Technology Project at Southwest United Graduate School (202302AP370002), National Natural Science Fund of China (42277236), Yunnan Fundamental Research Projects (202201BE070001-012), and Yunnan Major Scientific and Technological Projects (202202AG050019).

Data availability

The datasets used or analyzed during the current study are available from the corresponding author upon reasonable request.

Declarations

Competing interests

Bo Pan is an EBM of the journal Biochar, and he was not involved in the peer-review or handling of the manuscript. The authors have no other competing interests to disclose.

Author details

[1]Yunnan Provincial Key Laboratory of Soil Carbon Sequestration and Pollution Control, Faculty of Environmental Science & Engineering, Kunming University of Science & Technology, Kunming 650500, China. [2]College of Environmental Sciences and Engineering, Peking University, Beijing 100871, China. [3]Southwest United Graduate School, Kunming 650092, China. [4]Faculty of Modern Agricultural Engineering, Kunming University of Science and Technology, Kunming 650500, Yunnan, China.

Received: 25 April 2025 Revised: 30 October 2025 Accepted: 2 November 2025
Published online: 18 February 2026

References

Aeschbacher M, Sander M, Schwarzenbach RP (2010) Novel electrochemical approach to assess the redox properties of humic substances. Environ Sci Technol 44:87–93. https://doi.org/10.1021/es902627p

Akhoury A, Bromberg L, Hatton TA (2013) Interplay of electron hopping and bounded diffusion during charge transport in redox polymer electrodes. J Phys Chem B 117:333–342. https://doi.org/10.1021/jp302157g

Ameloot N, Graber ER, Verheijen FGA, De Neve S (2013) Interactions between biochar stability and soil organisms: review and research needs. Eur J Soil Sci 64:379–390. https://doi.org/10.1111/ejss.12064

Baker LL, Strawn DG, Rember WC, Sprenke KF (2011) Metal content of charcoal in mining-impacted wetland sediments. Sci Total Environ 409:588–594. https://doi.org/10.1016/j.scitotenv.2010.10.038

Bird MI, Wynn JG, Saiz G, Wurster CM, McBeath A (2015) The pyrogenic carbon cycle. Annu Rev Earth Planet Sci 43:273–298. https://doi.org/10.1146/annurev-earth-060614-105038

Çetin B, Büyükkoçak S, Zeinali S, Özer B (2013) Simulation of an integrated microfluidic device for bioparticle wash, separation and concentration. In: ASME 2013 4th international conference on micro/nanoscale heat and mass transfer.

Chacón FJ, Cayuela ML, Roig A, Sánchez-Monedero MA (2017) Understanding, measuring and tuning the electrochemical properties of biochar for environmental applications. Rev Environ Sci Bio/technol 16:695–715. https://doi.org/10.1007/s11157-017-9450-1

Chang R, Sohi SP, Jing F, Liu Y, Chen J (2019) A comparative study on biochar properties and Cd adsorption behavior under effects of ageing processes of leaching, acidification and oxidation. Environ Pollut 254:113123. https://doi.org/10.1016/j.envpol.2019.113123

Costantini A, Venezia V, Pota G, Bifulco A, Califano V, Sannino F (2020) Adsorption of cellulase on wrinkled silica nanoparticles with enhanced inter-wrinkle distance. Nanomaterials. https://doi.org/10.3390/nano10091799

Dasgupta D, Demichelis F, Tagliaferro A (1991) Electrical conductivity of amorphous carbon and amorphous hydrogenated carbon. Philos Mag B 63:1255–1266. https://doi.org/10.1080/13642819108205558

Dong X, Li G, Lin Q, Zhao X (2017) Quantity and quality changes of biochar aged for 5years in soil under field conditions. CATENA 159:136–143. https://doi.org/10.1016/j.catena.2017.08.008

Eckert H, Chen CJ, Greenblatt M, Herber RH (1988) Electron hopping in lithiated spinels: a temperature dependent Mössbauer study. J Phys Chem Solids 49:71–77. https://doi.org/10.1016/0022-3697(88)90137-0

Fan Q, Sun J, Chu L, Cui L, Quan G, Yan J, Hussain Q, Iqbal M (2018) Effects of chemical oxidation on surface oxygen-containing functional groups and adsorption behavior of biochar. Chemosphere 207:33–40. https://doi.org/10.1016/j.chemosphere.2018.05.044

Gámiz B, Velarde P, Spokas KA, Celis R, Cox L (2019) Changes in sorption and bioavailability of herbicides in soil amended with fresh and aged biochar. Geoderma 337:341–349. https://doi.org/10.1016/j.geoderma.2018.09.033

Gao D, Bai E, Yang Y, Zong S, Hagedorn F (2021) A global meta-analysis on freeze-thaw effects on soil carbon and phosphorus cycling. Soil Biol Biochem 159:108283. https://doi.org/10.1016/j.soilbio.2021.108283

Gu Y, Srikanth V, Salazar-Morales AI, Jain R, O'Brien JP, Yi SM, Soni RK, Samatey FA, Yalcin SE, Malvankar NS (2021) Structure of *Geobacter* pili reveals secretory rather than nanowire behaviour. Nature 597:430–434. https://doi.org/10.1038/s41586-021-03857-w

Hale S, Hanley K, Lehmann J, Zimmerman A, Cornelissen G (2011) Effects of chemical, biological, and physical aging as well as soil addition on the sorption of pyrene to activated carbon and biochar. Environ Sci Technol 45:10445–10453. https://doi.org/10.1021/es202970x

He L, Shan J, Zhao X, Wang S, Yan X (2019) Variable responses of nitrification and denitrification in a paddy soil to long-term biochar amendment and short-term biochar addition. Chemosphere 234:558–567. https://doi.org/10.1016/j.chemosphere.2019.06.038

Helmbold A, Hammer P, Thiele JU, Rohwer K, Meissner D (1995) Electrical conductivity of amorphous hydrogenated carbon. Philos Mag B 72:335–350. https://doi.org/10.1080/13642819508239088

Jackson NE, Savoie BM, Kohlstedt KL, Olvera de la Cruz M, Schatz GC, Chen LX, Ratner MA (2013) Controlling conformations of conjugated polymers and small molecules: the role of nonbonding interactions. J Am Chem Soc 135:10475–10483. https://doi.org/10.1021/ja403667s

Kappler A, Wuestner ML, Ruecker A, Harter J, Halama M, Behrens S (2014) Biochar as an electron shuttle between bacteria and Fe(III) minerals. Environ Sci Technol Lett 1:339–344. https://doi.org/10.1021/ez5002209

Klüpfel L, Keiluweit M, Kleber M, Sander M (2014) Redox properties of plant biomass-derived black carbon (biochar). Environ Sci Technol 48:5601–5611. https://doi.org/10.1021/es500906d

Kuhlbusch TAJ, Crutzen PJ (1995) Toward a global estimate of black carbon in residues of vegetation fires representing a sink of atmospheric CO_2 and a source of O_2. Glob Biogeochem Cycles 9:491–501. https://doi.org/10.1029/95GB02742

Li Z, Mao J, Chu W, Xu W (2019) Probing the surface reactivity of pyrogenic carbonaceous material (PCM) through synthesis of PCM-like conjugated microporous polymers. Environ Sci Technol 53:7673–7682. https://doi.org/10.1021/acs.est.9b01772

Li S, Shao L, Zhang H, He P, Lü F (2020) Quantifying the contributions of surface area and redox-active moieties to electron exchange capacities of biochar. J Hazard Mater 394:122541. https://doi.org/10.1016/j.jhazmat.2020.122541

Liu L, Fan S (2022) Effects of physical and chemical aging on polycyclic aromatic hydrocarbon (PAH) content and potential toxicity in rice straw biochars. Environ Sci Pollut Res 29:57479–57489. https://doi.org/10.1007/s11356-022-19869-6

Lv P, Jia C, Wei C, Zhao H, Chen R (2024) Biochar modulates intracellular electron transfer for nitrate reduction in denitrifying anaerobic methane oxidizing archaea. Bioresour Technol 406:130998. https://doi.org/10.1016/j.biortech.2024.130998

Lyu Q, Chen X, Zhang Y, Yu H, Han L, Xiao W (2021) One-pot fractionation of corn stover with peracetic acid and maleic acid. Bioresour Technol 320:124306. https://doi.org/10.1016/j.biortech.2020.124306

Mia S, Dijkstra FA, Singh B (2017) Chapter one - long-term aging of biochar: a molecular understanding with agricultural and environmental implications. Academic Press, pp 1–51

Miccoli I, Edler F, Pfnür H, Tegenkamp C (2015) The 100th anniversary of the four-point probe technique: the role of probe geometries in isotropic and anisotropic systems. J Phys Condens Matter 27:223201. https://doi.org/10.1088/0953-8984/27/22/223201

Mohan D, Pittman CU, Bricka M, Smith F, Yancey B, Mohammad J, Steele PH, Alexandre-Franco MF, Gómez-Serrano V, Gong H (2007) Sorption of arsenic, cadmium, and lead by chars produced from fast pyrolysis of wood and bark during bio-oil production. J Colloid Interface Sci 310:57–73. https://doi.org/10.1016/j.jcis.2007.01.020

Nie T, Hao P, Zhao Z, Zhou W, Zhu L (2019) Effect of oxidation-induced aging on the adsorption and co-adsorption of tetracycline and Cu^{2+} onto biochar. Sci Total Environ 673:522–532. https://doi.org/10.1016/j.scitotenv.2019.04.089

Prado A, Berenguer R, Esteve-Núñez A (2019) Electroactive biochar outperforms highly conductive carbon materials for biodegrading pollutants by enhancing microbial extracellular electron transfer. Carbon 146:597–609. https://doi.org/10.1016/j.carbon.2019.02.038

Prévoteau A, Ronsse F, Cid I, Boeckx P, Rabaey K (2016) The electron donating capacity of biochar is dramatically underestimated. Sci Rep 6:32870. https://doi.org/10.1038/srep32870

Quan G, Fan Q, Zimmerman AR, Sun J, Cui L, Wang H, Gao B, Yan J (2020) Effects of laboratory biotic aging on the characteristics of biochar and its water-soluble organic products. J Hazard Mater 382:121071. https://doi.org/10.1016/j.jhazmat.2019.121071

Rechberger MV, Kloss S, Rennhofer H, Tintner J, Watzinger A, Soja G, Lichtenegger H, Zehetner F (2017) Changes in biochar physical and chemical properties: accelerated biochar aging in an acidic soil. Carbon 115:209–219. https://doi.org/10.1016/j.carbon.2016.12.096

Reisser M, Purves RS, Schmidt MWI, Abiven S (2016) Pyrogenic carbon in soils: a literature-based inventory and a global estimation of its content in soil organic carbon and stocks. Front Earth Sci. https://doi.org/10.3389/feart.2016.00080

Saeed E, Piñeiro MM, Hermida-Merino C, Pastoriza-Gallego MJ (2019) Determination of transport properties of glycol-based nanofluids derived from surface functionalized graphene. Nanomaterials 9:252. https://doi.org/10.3390/nano9020252

Saha N, Xin D, Chiu PC, Reza MT (2019) Effect of pyrolysis temperature on acidic oxygen-containing functional groups and electron storage capacities of pyrolyzed hydrochars. ACS Sustain Chem Eng 7:8387–8396. https://doi.org/10.1021/acssuschemeng.9b00024

Santín C, Doerr SH, Kane ES, Masiello CA, Ohlson M, de la Rosa JM, Preston CM, Dittmar T (2016) Towards a global assessment of pyrogenic carbon from vegetation fires. Glob Change Biol 22:76–91. https://doi.org/10.1111/gcb.12985

Saquing JM, Yu Y-H, Chiu PC (2016) Wood-derived black carbon (biochar) as a microbial electron donor and acceptor. Environ Sci Technol Lett 3:62–66. https://doi.org/10.1021/acs.estlett.5b00354

Schievano A, Berenguer R, Goglio A, Bocchi S, Marzorati S, Rago L, Louro RO, Paquete CM, Esteve-Núñez A (2019) Electroactive biochar for large-scale environmental applications of microbial electrochemistry. ACS Sustain Chem Eng 7:18198–18212. https://doi.org/10.1021/acssuschemeng.9b04229

Schmidt MWI, Noack AG (2000) Black carbon in soils and sediments: analysis, distribution, implications, and current challenges. Glob Biogeochem Cycles 14:777–793. https://doi.org/10.1029/1999GB001208

Shang Z, Ren D, Yang F, Wang J, Liu B, Chen F, Du Y (2024) Simultaneous immobilization of V and Cr availability, speciation in contaminated soil and accumulation in ryegrass by using Fe-modified pyrolysis char. J Hazard Mater 469:134097. https://doi.org/10.1016/j.jhazmat.2024.134097

Si D, Wu H, Yang M, Fan T, Wang D, Chen L, Zhu C, Fang G, Wu S, Zhou D (2023) Linking pyrogenic carbon redox property to arsenite oxidation: impact of N-doping and pyrolysis temperature. J Hazard Mater 445:130477. https://doi.org/10.1016/j.jhazmat.2022.130477

Sun T, Levin BDA, Guzman JJL, Enders A, Muller DA, Angenent LT, Lehmann J (2017) Rapid electron transfer by the carbon matrix in natural pyrogenic carbon. Nat Commun 8:14873. https://doi.org/10.1038/ncomms14873

Sun T, Levin BDA, Schmidt MP, Guzman JJL, Enders A, Martínez CE, Muller DA, Angenent LT, Lehmann J (2018) Simultaneous quantification of electron transfer by carbon matrices and functional groups in pyrogenic carbon. Environ Sci Technol 52:8538–8547. https://doi.org/10.1021/acs.est.8b02340

Sun T, Guzman JJL, Seward JD, Enders A, Yavitt JB, Lehmann J, Angenent LT (2021) Suppressing peatland methane production by electron snorkeling through pyrogenic carbon in controlled laboratory incubations. Nat Commun 12:4119. https://doi.org/10.1038/s41467-021-24350-y

Tan L, Ma Z, Yang K, Cui Q, Wang K, Wang T, Wu G-L, Zheng J (2020) Effect of three artificial aging techniques on physicochemical properties and Pb adsorption capacities of different biochars. Sci Total Environ 699:134223. https://doi.org/10.1016/j.scitotenv.2019.134223

Varga M, Izak T, Vretenar V, Kozak H, Holovsky J, Artemenko A, Hulman M, Skakalova V, Lee DS, Kromka A (2017) Diamond/carbon nanotube composites: raman, FTIR and XPS spectroscopic studies. Carbon 111:54–61. https://doi.org/10.1016/j.carbon.2016.09.064

Wang X, Zhou W, Liang G, Song D, Zhang X (2015) Characteristics of maize biochar with different pyrolysis temperatures and its effects on organic carbon, nitrogen and enzymatic activities after addition to fluvo-aquic soil. Sci Total Environ 538:137–144. https://doi.org/10.1016/j.scitotenv.2015.08.026

Wang Y, Zhang W, Shang J, Shen C, Joseph SD (2019) Chemical aging changed aggregation kinetics and transport of biochar colloids. Environ Sci Technol 53:8136–8146. https://doi.org/10.1021/acs.est.9b00583

Wang L, O'Connor D, Rinklebe J, Ok YS, Tsang DCW, Shen Z, Hou D (2020) Biochar aging: mechanisms, physicochemical changes, assessment, and implications for field applications. Environ Sci Technol 54:14797–14814. https://doi.org/10.1021/acs.est.0c04033

Wang L, Gao C, Yang K, Sheng Y, Xu J, Zhao Y, Lou J, Sun R, Zhu L (2021) Effects of biochar aging in the soil on its mechanical property and performance for soil CO_2 and N_2O emissions. Sci Total Environ 782:146824. https://doi.org/10.1016/j.scitotenv.2021.146824

Wang S, Cheng A, Liu F, Zhang J, Xia T, Zeng X, Fan W, Zhang Y (2023) Catalytic conversion network for lignocellulosic biomass valorization: a panoramic view. Ind Chem Mater 1:188–206. https://doi.org/10.1039/D2IM00054G

Wu C, Liu X, Wu X, Dong F, Xu J, Zheng Y (2019) Sorption, degradation and bioavailability of oxyfluorfen in biochar-amended soils. Sci Total Environ 658:87–94. https://doi.org/10.1016/j.scitotenv.2018.12.059

Wu Y, Tan Z, Zhou T, Wang Z, Xue Z, Yan Y, He H, Pan J (2025) Regulation mechanisms of biochar-derived endogenous substances on heavy metal mobility in the soil-crop system: a critical review. Environ Res 285:122557. https://doi.org/10.1016/j.envres.2025.122557

Xu W, Pignatello JJ, Mitch WA (2013) Role of black carbon electrical conductivity in mediating hexahydro-1,3,5-trinitro-1,3,5-triazine (RDX) transformation on carbon surfaces by sulfides. Environ Sci Technol 47:7129–7136. https://doi.org/10.1021/es4012367

Xu S, Adhikari D, Huang R, Zhang H, Tang Y, Roden E, Yang Y (2016) Biochar-facilitated microbial reduction of hematite. Environ Sci Technol 50:2389–2395. https://doi.org/10.1021/acs.est.5b05517

Yang F, Zhao L, Gao B, Xu X, Cao X (2016) The interfacial behavior between biochar and soil minerals and its effect on biochar stability. Environ Sci Technol 50:2264–2271. https://doi.org/10.1021/acs.est.5b03656

Yuan Y, Bolan N, Prévoteau A, Vithanage M, Biswas JK, Ok YS, Wang H (2017) Applications of biochar in redox-mediated reactions. Bioresour Technol 246:271–281. https://doi.org/10.1016/j.biortech.2017.06.154

Yuan J, Wen Y, Dionysiou DD, Sharma VK, Ma X (2022) Biochar as a novel carbon-negative electron source and mediator: electron exchange capacity (EEC) and environmentally persistent free radicals (EPFRs): a review. Chem Eng J 429:132313. https://doi.org/10.1016/j.cej.2021.132313

Zhang S, Yang X, Ju M, Liu L, Zheng K (2019) Mercury adsorption to aged biochar and its management in China. Environ Sci Pollut Res Int 26:4867–4877. https://doi.org/10.1007/s11356-018-3945-3

Zhao R, Coles N, Wu J (2015) Carbon mineralization following additions of fresh and aged biochar to an infertile soil. CATENA 125:183–189. https://doi.org/10.1016/j.catena.2014.10.026

Zhao Z, Zhang Y, Holmes DE, Dang Y, Woodard TL, Nevin KP, Lovley DR (2016) Potential enhancement of direct interspecies electron transfer for syntrophic metabolism of propionate and butyrate with biochar in up-flow anaerobic sludge blanket reactors. Bioresour Technol 209:148–156. https://doi.org/10.1016/j.biortech.2016.03.005

Zhao Z, Cao Y, Li S, Zhang Y (2021) Effects of biowaste-derived biochar on the electron transport efficiency during anaerobic acid orange 7 removal. Bioresour Technol 320:124295. https://doi.org/10.1016/j.biortech.2020.124295

Zhao K, Wang X, Li B, Shang J (2023) The roles of Fe oxyhydroxide coating and chemical aging in pyrogenic carbon nanoparticle transport in unsaturated porous media. Environ Pollut 317:120776. https://doi.org/10.1016/j.envpol.2022.120776

Zhu X, Chen B, Zhu L, Xing B (2017) Effects and mechanisms of biochar-microbe interactions in soil improvement and pollution remediation: a review. Environ Pollut 227:98–115. https://doi.org/10.1016/j.envpol.2017.04.032